environmental microbiology

Environmental Microbiology (2020) **22**(4), 1397–1408 doi:10.1111/1462-2920.14955

Carbon substrate re-orders relative growth of a bacterium using Mo-, V-, or Fe-nitrogenase for nitrogen fixation

Katja E. Luxem,[1] Anne M. L. Kraepiel,[2] Lichun Zhang,[3] Jacob R. Waldbauer [3] and Xinning Zhang [1,2*]

[1]*Department of Geosciences, Princeton University, Princeton, NJ, 08544, USA.*

[2]*Princeton Environmental Institute, Princeton University, Princeton, NJ, 08544, USA.*

[3]*Department of the Geophysical Sciences, University of Chicago, Chicago, IL, 60637, USA.*

Summary

Biological nitrogen fixation is catalyzed by the molybdenum (Mo), vanadium (V) and iron (Fe)-only nitrogenase metalloenzymes. Studies with purified enzymes have found that the 'alternative' V- and Fe-nitrogenases generally reduce N_2 more slowly and produce more byproduct H_2 than the Mo-nitrogenase, leading to an assumption that their usage results in slower growth. Here we show that, in the metabolically versatile photoheterotroph *Rhodopseudomonas palustris*, the type of carbon substrate influences the relative rates of diazotrophic growth based on different nitrogenase isoforms. The V-nitrogenase supports growth as fast as the Mo-nitrogenase on acetate but not on the more oxidized substrate succinate. Our data suggest that this is due to insufficient electron flux to the V-nitrogenase isoform on succinate compared with acetate. Despite slightly faster growth based on the V-nitrogenase on acetate, the wild-type strain uses exclusively the Mo-nitrogenase on both carbon substrates. Notably, the differences in H_2:N_2 stoichiometry by alternative nitrogenases (~1.5 for V-nitrogenase, ~4–7 for Fe-nitrogenase) and Mo-nitrogenase (~1) measured here are lower than prior *in vitro* estimates. These results indicate that the metabolic costs of V-based nitrogen fixation could be less significant for growth than previously assumed, helping explain why alternative nitrogenase genes persist in diverse diazotroph lineages and are broadly distributed in the environment.

Introduction

Biological nitrogen fixation has sustained ecosystem fertility and primary production throughout Earth history. This fundamental prokaryotic process reduces atmospheric dinitrogen (N_2) to ammonia (NH_3) in a metabolically costly reaction catalysed by the metalloenzyme nitrogenase (Nase). There are three phylogenetically and structurally distinct isoforms of Nase: the molybdenum (Mo-) and 'alternative' vanadium (V-) and iron (Fe-) only Nases (Eady, 1996). These can be differentiated by a key active site metal atom (Mo, V, or Fe) in addition to their kinetics, stable isotope fractionation and reaction stoichiometry (Bishop *et al*., 1986; Robson *et al*., 1986; Eady, 1996; Gosse *et al*., 2010; McKinlay and Harwood, 2010b; Zhang *et al*., 2014; Mus *et al*., 2018). The metabolic costs of Mo-based diazotrophy are well characterized, including the direct energy and reducing power requirements of N_2 fixation and indirect costs related to oxygen protection (Andersen and Shanmugam, 1977; McKinlay and Harwood, 2010b; Großkopf and LaRoche, 2012; Inomura *et al*., 2016). The Mo-Nase is considered the most efficient isoform and the primary form responsible for N_2 fixation in the environment. However, alternative V- and Fe-Nase genes are widespread (Betancourt *et al*., 2008; McRose *et al*., 2017) and active (Hodkinson *et al*., 2014; Zhang *et al*., 2016; Darnajoux *et al*., 2017, 2019; McRose *et al*., 2017) in diverse taxa and environments, prompting questions on their roles in ecosystem nitrogen and trace metal cycling. To better understand the persistence of Nase diversity and the controls on environmental N_2 fixation, it is necessary to study how alternative N_2 fixation affects the growth physiology of diazotrophs (Glazer *et al*., 2015).

Compared with the Mo-Nase, less is known about the cellular costs of alternative V- and Fe-Nase-based diazotrophy. All Nase isoforms produce H_2 as an obligatory byproduct of N_2 reduction (Simpson and Burris, 1984; Harris *et al*., 2018a; Harris *et al*., 2018b). Early *in vitro*

Received 3 October, 2019; accepted 7 February, 2020. *For correspondence. E-mail xinningz@princeton.edu; Tel. (609) 258-2489.

data indicated that the alternative V- and Fe-Nases produce more H_2 than the Mo-Nase, resulting in greater energy and reducing power requirements (Eady, 1996). It has also been suggested that V- and Fe-only dependent diazotrophy are more oxygen (O_2) sensitive than Mo-based diazotrophy (Robson *et al*., 1986; Krahn *et al*., 1996), possibly leading to greater indirect metabolic costs or more restrictive anaerobic lifestyles. These findings are consistent with observations that all diazotrophic organisms possess the Mo-Nase (Dos Santos *et al*., 2012) and only use the alternative Nases under Mo limited conditions or genetic Mo-Nase inactivation (Jacobson *et al*., 1986; Luque and Pau, 1991; Schneider *et al*., 1991; Gollan *et al*., 1993; Oda *et al*., 2005; Hamilton *et al*., 2011; Demtröder *et al*., 2019). However, the effects of these observations on organism fitness remain poorly characterized, and the assumption that Mo-based diazotrophy is always superior is challenged by field experiments demonstrating that several diazotrophic isolates grew faster in the presence of vanadium than molybdenum (Betancourt *et al*., 2008).

Here, we investigate the ability of the V- and Fe-Nases to fulfill nitrogen requirements and enable competitive growth under photoheterotrophic conditions in a genetically tractable model organism, *Rhodopseudomonas palustris* CGA009 (Larimer *et al*., 2004). During photoheterotrophic growth, light is the source of energy and organic substrates are the source of carbon and reductant for biosynthesis. Reductant in cellular electron carrier pools (e.g. NAD(P)H and reduced ubiquinone) accumulates during oxidative processing of organic substrates (Fig. 1, Arrow B) when external electron acceptors are absent (Fig. 1, Arrow G). To maintain redox homeostasis and enable continued substrate assimilation, these reductants must be re-oxidized through direct biomass synthesis (Fig. 1, Arrow D), Nase activity (Fig. 1, Arrow F), or re-fixation of some of the CO_2 produced during substrate assimilation (Fig. 1, Arrow E), such that electrons from the organic substrate are fully allocated between biomass, H_2 and CO_2. Under these conditions, Nase is important both for nutrient acquisition and as an electron sink (Muller, 1933; Hillmer and Gest, 1977; McKinlay and Harwood, 2010a, 2011; Farmer *et al*., 2014; Gordon and McKinlay, 2014; McCully and McKinlay, 2016). To determine how simultaneous nitrogen acquisition and electron balancing constraints influence growth based on each Nase isoform, we cultured wild type *R. palustris* and mutant strains known to utilize only a single isoform (hereafter Mo-Nase, V-Nase and Fe-Nase strains, Oda *et al*., 2005) in diazotrophic photoheterotrophic media with organic substrates of varying oxidation states and assimilation pathways (Table 1) and measured growth, N_2 and CO_2 fixation, H_2 production, biomass composition and global protein abundance patterns. Our results demonstrate and explain why, depending on the carbon substrate, the alternative V-Nase isoform can support photoheterotrophic growth as fast as the Mo-Nase isoform.

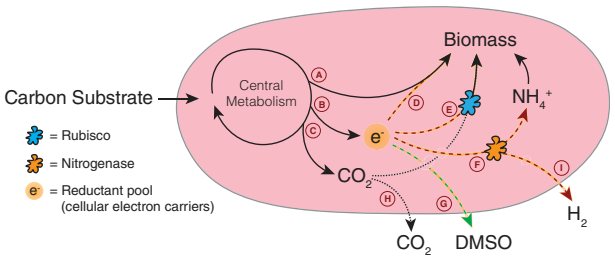

Fig. 1. Electron balancing processes used by *R. palustris* during diazotrophic, photoheterotrophic growth. During photoheterotrophic growth, *R. palustris* consumes carbon substrates and converts them into biomass precursors and CO_2 ('central metabolism,' arrows A and C, respectively). This process reduces cellular electron carriers (arrow B), which must be re-oxidized to maintain intracellular redox homeostasis and thereby enable continued carbon substrate assimilation. The electron sinks that stabilize the cellular electron pool are re-fixation of some of the CO_2 produced during substrate assimilation (arrow E), synthesis of certain biomass precursors (arrow D), and Nase activity (arrow F). To achieve redox homeostasis, substrate-derived electrons must be fully allocated between biomass, H_2 (arrow I) and CO_2 (arrow H). The cellular electron pool can also be re-oxidized by extracellular electron acceptors like dimethyl sulfoxide (DMSO, arrow G).

Results and discussion

Alternative V-Nase can support diazotrophic growth as fast as the Mo-Nase on acetate

Previous studies have shown that photoheterotrophic growth of *R. palustris* on succinate, acetate, and butyrate is associated with increasing cellular electron burden and redox stress (McKinlay and Harwood, 2011). To determine how these substrates influence growth based on different Nase isoforms, we compared the

Table 1. Oxidation states of *R. palustris* biomass and carbon substrates.

Substrate	Formula	Oxidation state[a]
Succinate	$C_4H_6O_4$	+0.5
Acetate	$C_2H_4O_2$	0
Measured biomass[b]	$CH_{1.75}N_{0.18}O_{0.54}$	−0.13
Published biomass[c]	$CH_{1.8}N_{0.18}O_{0.38}$	−0.5
Butyrate	$C_4H_8O_2$	−1

a. Average oxidation state of carbon in the compound calculated according to Dick (2014).
b. Average biomass composition of all strains on succinate and acetate.
c. The elemental composition of *R. palustris* 42OL during photoheterotrophic growth with acetate and ammonium (Carlozzi and Sacchi, 2001).

growth of the wild type strain, which fixed nitrogen exclusively with the Mo-Nase isoform in all three carbon substrates (see Supporting Information Discussion and Figs S1, S2, and S3), with that of mutant strains using exclusively the V- or Fe-Nase. In our experiments, when provided with succinate as the carbon and electron source, the V-Nase strain grew ~20% slower than the Mo-Nase utilizing wild type strain ($0.57 \pm 0.02\ day^{-1}$ vs. $0.70 \pm 0.01\ day^{-1}$, $p < 10^{-5}$, errors are SE, Fig. 2). Similarly, in the mixed butyrate-bicarbonate treatment, which combines a very reduced and oxidized carbon substrate, the V-Nase strain grew ~20% slower than the wild type strain ($0.66 \pm 0.01\ day^{-1}$ vs. $0.82 \pm 0.02\ day^{-1}$, $p \sim 10^{-8}$). These growth rate patterns are consistent with prior observations (Oda *et al*., 2005) and the general view that nitrogen fixation with the Mo-Nase isoform yields the fastest growth. In contrast, when provided with acetate, we found that the V-Nase strain grew ~10% faster than Mo-Nase utilizing wild type strain ($0.80 \pm 0.01\ day^{-1}$ vs. $0.74 \pm 0.01\ day^{-1}$, $p = 10^{-2}$). The V-Nase strain also had a higher maximal optical density (OD_{660}) than the wild type strain for growth on acetate but not succinate (Fig. S4). To our knowledge, these are the first data showing that, depending on the carbon substrate, diazotrophic growth with the alternative V-Nase can rival growth based on the canonical Mo-Nase isoform.

Metabolic conditions influence the rate of N_2 reduction by the V-Nase isoform

To understand why the V-Nase isoform enables growth comparable to the Mo-Nase isoform on some carbon substrates but not others, we measured biomass composition (Fig. 3), CO_2 and N_2 fixation rates (Fig. 4), and global protein abundance patterns on acetate and

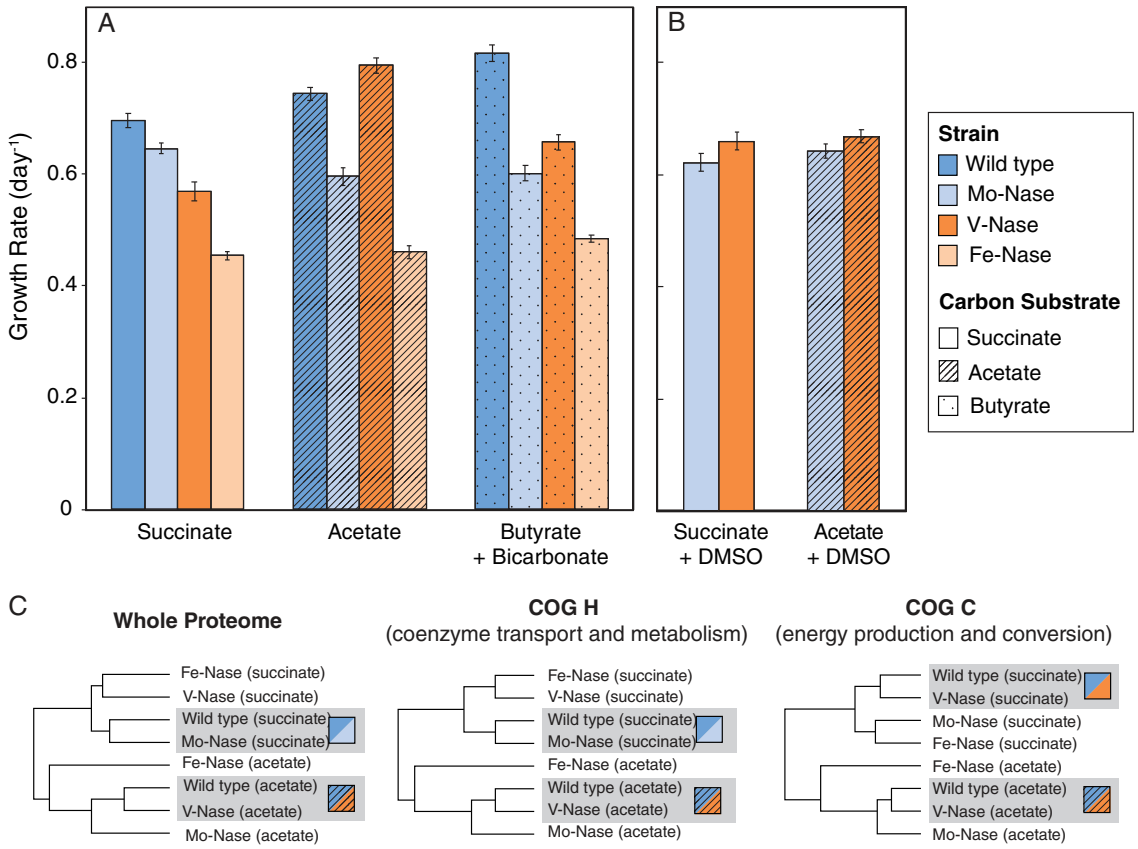

Fig. 2. A. *R. palustris* growth rates. The wild type strain, which uses the Mo-Nase isoform, grows fast in all treatments. The V-Nase strain grows faster than the Mo-Nase utilizing wild type strain when provided with the more reduced carbon substrate, acetate, but not with the more oxidized substrate, succinate. It also grows faster than the Mo-Nase mutant strain on acetate and butyrate + bicarbonate. B. Growth rate differences are linked to electron balance. The addition of an external electron acceptor, dimethyl sulfoxide (DMSO), diminishes the growth advantage of the V-Nase strain on the more reduced carbon substrate acetate. In the absence of DMSO, the growth rates are significantly different within each carbon treatment ($p < 0.05$). However, in the presence of DMSO, the growth rates of the Mo- and V-Nase strains are not significantly different. The error bars show the mean ± SE. C. *R. palustris* protein abundance dendrograms. Hierarchical clustering of all detected proteins and of the proteins annotated to COG H (coenzyme transport and metabolism) mimics the observed growth rate trends, demonstrating that, physiologically, on acetate, the wild-type strain is more similar to the V-Nase strain than the Mo-Nase strain. From an energy acquisition perspective (COG C), the wild-type strain is more similar to the V-Nase strain than the Mo-Nase strain on both succinate and acetate.

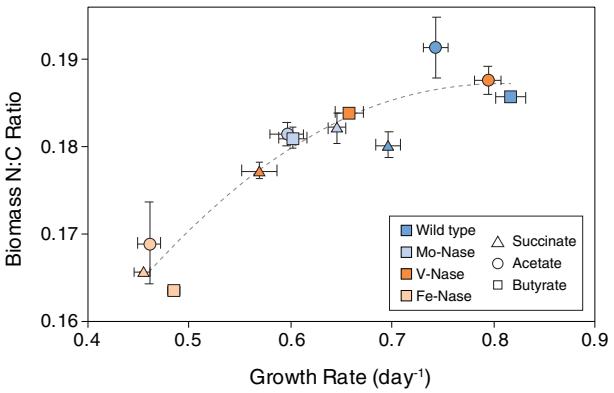

Fig. 3. *R. palustris* biomass composition. The fastest-growing strains are also the most nitrogen rich. The wild type and V-Nase strains adjust their growth rates depending on the carbon substrate, whereas the Fe- and Mo-Nase strains grow at similar rates in all treatments. Error bars show the mean ± SE.

succinate for all strains. Despite indistinguishable V-Nase protein abundance (Fig. S1; log2 abundance difference < 0.3, $p > 0.3$ for VnfHDKG), the V-Nase strain reduces N_2 approximately 30% more slowly on succinate than on acetate (Fig. 4, $p = 0.31$). Its biomass N:C ratio is comparable to the wild type strain on acetate but is substantially lower on succinate (Fig. 3). This is notable because, in our experiments, higher biomass N:C ratios are associated with faster growth (Fig. 3), suggesting that the growth limiting process is either nitrogen acquisition itself and/or a process correlated with nitrogen acquisition, such as electron availability and balance. Importantly, there were no statistically significant differences in Nase abundance between growth on succinate and acetate for all strains (Fig. S1), demonstrating that the observed growth rate trends are due to differences in the rate and efficiency of the enzyme and its integration into metabolism rather than Nase abundance. The different growth pattern and N_2 reduction rate of the V-Nase strain on acetate and succinate relative to the Mo-Nase utilizing wild type strain demonstrate that the carbon substrate used for growth can alter the relative rate of nitrogen acquisition by the V-Nase isoform.

Mo-Nase strain grows slowly compared with the wild type strain

We also grew a Mo-Nase mutant strain. This strain grew ~10% more slowly than the wild type strain when succinate was the carbon source (0.65 ± 0.01 day^{-1} vs. 0.70 ± 0.01, $p \sim 3 \times 10^{-3}$, Fig. 1). On acetate, it grew ~25% more slowly than the V-Nase strain (0.60 ± 0.02 day^{-1} vs. 0.80 ± 0.01 day^{-1}, $p < 10^{-9}$) and ~20% more slowly than the wild type strain (0.74 ± 0.01 day^{-1}, $p \sim 10^{-9}$). This result is surprising because the wild type strain uses exclusively the Mo-Nase to fix nitrogen (see Supporting Information Discussion), and the Mo-Nase strain mutations are in proteins that are not used by the wild type strain under these conditions (the alternative nitrogenase structural protein genes *vnfH* and *anfH*, Fig. S1). The Mo-Nase mutant strain has a somewhat lower abundance of several Mo-Nase accessory proteins (including NifW, NifS2 and NifA; Fig. S3) and higher abundance of glutamate and ammonium transporters (Fig. S5) relative to the wild type strain, possibly indicating altered intracellular fixed nitrogen availability. We cannot exclude the possibility that there are additional random mutations in the Mo-Nase strain compared with the wild type strain, although similar growth phenotypes and gene expression profiles were previously observed for these strains during growth on succinate at 30°C (Oda *et al*., 2005). Thus, the reasons for the different growth rates of these strains in our experiments are unclear. From a mechanistic perspective, the slow CO_2 re-fixation rate of the Mo-Nase strain on acetate is notable, which could be due to its lower, more oxidized, cellular [NADH]/[NAD$^+$] ratio (Fig. S6) and lower Form II Rubisco abundance on acetate (Fig. S5). This is consistent with measurements of particularly high bacteriochlorophyll *a* concentrations in the Mo-Nase strain (Figs. S5 and S7) and a lower ratio of the more efficient light-harvesting 4 (LH4) complex to the light-harvesting 2 (LH2) complex (Table S1, Fixen *et al*., 2019), which could reflect an insufficient rate of reverse electron flow to regenerate NADH for continued carbon assimilation (Hädicke *et al*., 2011). However, it remains unclear how mutations in the V-Nase *vnfH* and Fe-Nase *anfH* genes would cause this effect. Regardless of the underlying mechanism, the slow growth of the Mo-Nase strain on acetate demonstrates that the alternative nitrogenase genes are well integrated into the genome and possibly regulatory pathways of *R. palustris* CGA009 and that other metabolic constraints can be more important determinants of fitness than Mo- versus V-Nase isoform usage.

Diazotrophic growth on succinate and acetate are differentiated by electron availability

Previous *in vitro* studies have shown that electron availability, which can be manipulated by varying the dinitrogenase reductase versus dinitrogenase protein ratio, can influence the efficiency of Nase, including the specific N_2 reduction rate and the H_2:N_2 ratio (Eady, 1996; Harris *et al*., 2019). For *R. palustris*, the key determinants of whether it is limited by electron acceptors or donors are (i) the oxidation state of the substrate relative to the biomass (Table 1) and (ii) the pathway by which substrate is assimilated into biomass (McKinlay and

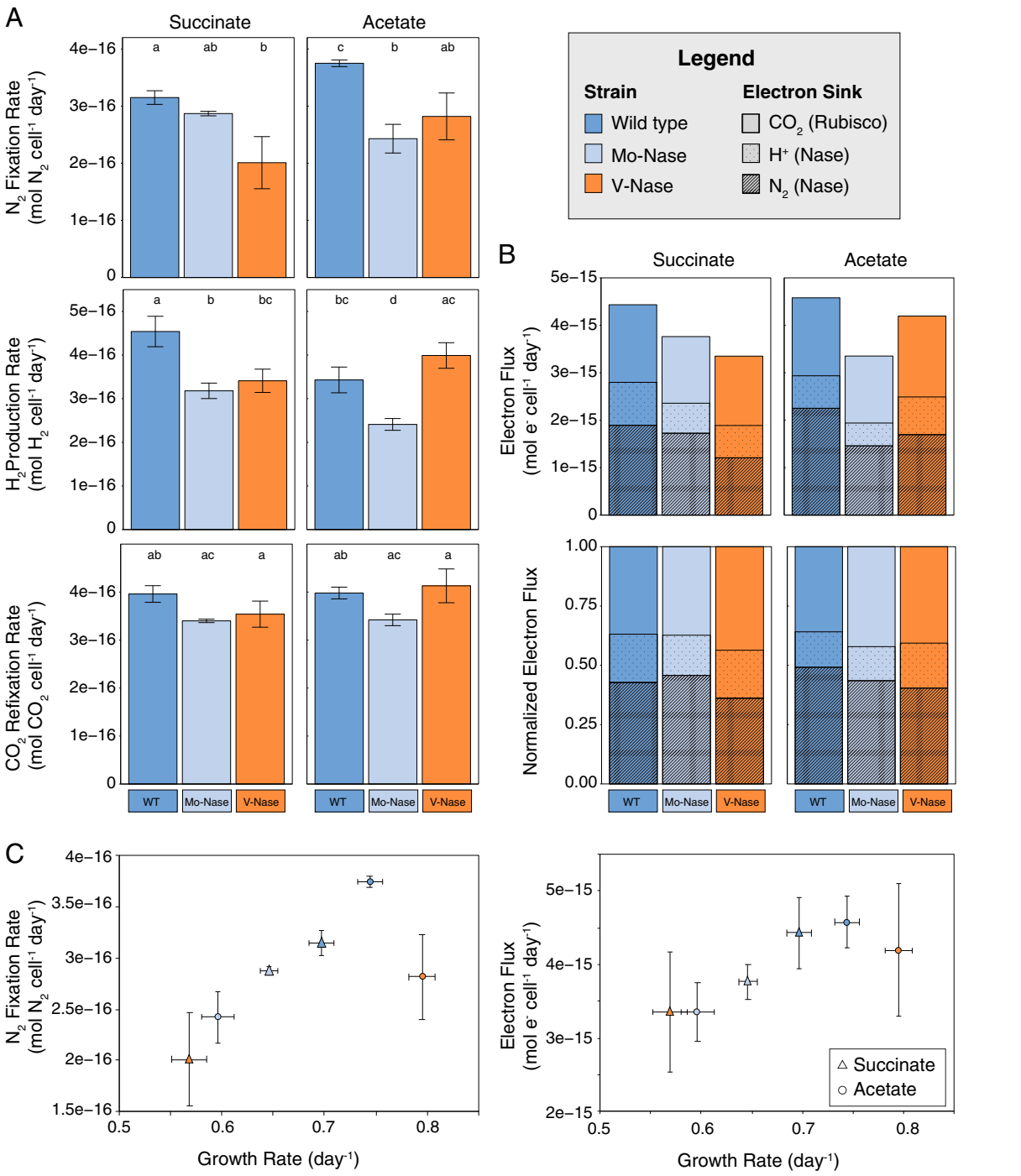

Fig. 4. A. Rates of N_2 and CO_2 fixation and H_2 production of *R. palustris* strains growing on succinate (left) and acetate (right). For H_2 production, the error bars represent the standard error of the slope when data from multiple biological replicates ($n \geq 2$) are plotted together. For CO_2 and N_2 fixation rates, the error bars represent the standard error of multiple biological replicates ($n \geq 2$). Different letters represent treatments that are significantly different at $p < 0.05$. B. Electron flux through Nase and Rubisco. The fraction of the electron flux through Nase versus Rubisco remains approximately constant despite differences in total flux and in the partitioning of electrons through Nase to proton versus N_2 reduction. C. Growth rate versus nitrogen fixation rate and total electron flux. The nitrogen fixation rate and the reductive electron flux through Nase and Rubisco scale with the growth rate. Error bars show the mean ± SE. Data for the Fe-Nase strain are provided in the Supporting Information.

Harwood, 2010a, 2011). Acetate is assimilated via the glyoxylate shunt (indicated in our data by high expression of isocitrate lyase in acetate-grown cells, Fig. S8), resulting in rapid electron availability for energy acquisition and carbon fixation in *R. palustris* (Alsiyabi *et al.*, 2019). In contrast, succinate is assimilated through the

oxidative TCA cycle, which is associated with greater CO_2 loss (McKinlay and Harwood, 2011) and reduced electron flow through the energy acquiring electron transport chain (Alsiyabi *et al*., 2019). Proteins related to branched-chain amino acid metabolism, whose synthesis can re-oxidize cellular electron carriers for *R. palustris* during photoheterotrophic growth on succinate but not on acetate (McCully *et al*., 2019), are more abundant in this treatment (Fig. S8). The similar abundance changes in a wide range of proteins related to carbon metabolism and electron balance (Fig. S8) demonstrate that, despite differences in Nase isozyme usage and growth rates, the metabolic shift from diazotrophic growth on succinate to acetate is broadly consistent between strains and compatible with a greater cellular electron burden during growth on acetate (McKinlay and Harwood, 2011).

Excess H_2 production by the V-Nase strain does not preclude fast growth

H_2 is an obligatory byproduct of biological N_2 fixation. *In vitro* experiments in the 1980s and 1990s led to the conclusion that the alternative V-Nase produces approximately threefold more H_2 per N_2 reduced than the Mo-Nase (Table 2; literature compilation in Table S2; Bishop *et al*., 1986; Dilworth *et al*., 1993; Eady, 1996; Schneider *et al*., 1997; Gosse *et al*., 2010; McKinlay and Harwood, 2010b; Mus *et al*., 2018). As the H_2:N_2 ratio increases, Nase supplies less fixed nitrogen relative to its contribution as an electron sink. This observation underpins the long-standing paradigm that use of the alternative Nases always results in slower diazotrophic growth than the Mo-Nase (Schubert and Evans, 1976; Eady, 1996).

To evaluate this hypothesis, we measured H_2 production in each treatment (Table 2; Fig. 4). During growth on succinate, our data are compatible with the classical view that excess H_2 production by the V-Nase strain leads to slower growth compared with the Mo-Nase utilizing strains. For example, it has a lower biomass N:C ratio despite a higher abundance of the primary electron donor to Nase, the ferredoxin protein Fer1 (log2 abundance difference of 0.53 $\pm$ 2.56 relative to the wild type strain, $p < 0.01$; Fixen *et al*., 2018). These data indicate that, on succinate, nitrogen acquisition is more limiting to growth than electron balance. In contrast, when grown on acetate, the V-Nase strain produced a similar amount of excess H_2 (Table 2) compared with the wild type strain, yet grew just as fast, demonstrating that excess H_2 production by the V-Nase isoform is not always disadvantageous for growth. The strong correlation between growth rate and both N_2 fixation rate and the total electron flux through Nase and Rubisco (Fig. 4C) for V- and Mo-based nitrogen fixation suggests that the tradeoff between nitrogen acquisition and electron balancing, which must be co-optimized for optimal growth, depends on broader metabolic conditions like electron availability. Taken together, our data show that the physiological impact of excess H_2 production on growth varies depending on the metabolic conditions.

Table 2. H_2:N_2 ratios in *R. palustris*.

	Succinate	Acetate	Literature[a]
Wild type strain	1.4 ± 0.3	0.9 ± 0.2	1
Mo-Nase strain	1.1 ± 0.2	1.0 ± 0.2	1
V-Nase strain	1.7 ± 0.6	1.4 ± 0.5	3
Fe-Nase strain[b]	6.9 ± 0.8	3.9 ± 0.4	7.5–9

The V-Nase strain has a lower H_2:N_2 ratio than reported previously. Errors are SEs. The differences between the wild type, Mo-Nase and V-Nase strains are not statistically significant.

a. See e.g. Eady (1996) and Gosse and colleagues (2010).

b. Fe-Nase ratio was calculated by adjusting $^{15}N_2$-fixation rates measured in serum vials to Balch Tubes by 1.5, the average difference between rates in serum vials and Balch tubes for the other strains (see Supporting Information Experimental Procedures).

In our experiments, H_2 production directly reflects Nase activity because there is no functional uptake hydrogenase in *R. palustris* CGA009 (Rey *et al*., 2006; confirmed with proteomics, see Supporting Information). Our direct measurements of N_2 reduction and H_2 production indicate that the V-Nase H_2:N_2 ratio can be as low as ~1.5, half of the canonical 3:1 ratio (Table 2). In fact, recent evidence has confirmed that all three forms of Nase use an analogous catalytic mechanism with the same minimum 1 H_2: 1 N_2 stoichiometry for N_2 binding to the active site (Lukoyanov *et al*., 2015, 2016; Harris *et al*., 2018b; Harris *et al*., 2019). Many of the measurements that led to the canonical 3:1 ratio for V-Nase were conducted at 30°C (Bishop *et al*., 1986; Dilworth *et al*., 1993) but there are hints that the H_2:N_2 ratio may be temperature dependent and that it is lower at 19°C, the temperature where our growth experiments were performed (Table S2; Miller and Eady, 1988). Additionally, as temperatures decrease, the V-Nase isoform's *in vitro* N_2 (Miller and Eady, 1988) and *in vivo* acetylene (Darnajoux, 2015) reduction rates decrease less than that of the Mo-Nase. This could help explain why Oda and colleagues (2005) observed a larger gap between V- and Mo-Nase based growth rates on succinate (~30%) than observed here (~20%). Thus, as suggested by Miller and Eady (1988) over three decades ago, temperature could be a key parameter modulating the relative favourability of fixing nitrogen with the Mo- or V-Nase isoforms.

Fe-Nase strain grows slowly because of excess H_2 production

Unlike the V-Nase strain, the Fe-Nase strain grew slowly on all three carbon substrates (0.45 $\pm$ 0.01 day^{-1} on

succinate, 0.46 ± 0.01 day^{-1} on acetate and 0.48 ± 0.01 day^{-1} on butyrate-bicarbonate). It produced much more H_2 than the other strains, accumulating up to 20% v/v H_2 in the culture headspace. Although it has a comparable total electron flux through Nase (Fig. S9), it has the lowest biomass N:C ratios of all strains and a much lower N_2 reduction rate (Fig. 3, Fig. S9C), demonstrating strong nitrogen limitation. In addition, the Fe-Nase strain has the lowest intracellular [NAD(P)H]/[NAD(P)$^+$] ratios (Fig. S6) and expresses more electron acquisition proteins than other strains, like formate dehydrogenase and the electron bifurcating protein complex FixABC used by organisms to maximize energy conservation (Fig. S5; also see Oda *et al*., 2005). These data indicate that the Fe-Nase isoform over-allocates electron flux to H_2 production at the expense of nitrogen acquisition, resulting in slower growth of the Fe-Nase strain relative to the other strains. In the environment, it is possible that this stark growth disadvantage could be mitigated by the presence of a functional uptake hydrogenase. Indeed, *R. palustris* CGA009 has a non-functional uptake hydrogenase due to a frameshift mutation in HupV (Rey *et al*., 2006), and early chemostat experiments with *Azotobacter vinelandii* showed similar growth rates on the Mo- and Fe-Nases when an uptake hydrogenase was present (Bishop *et al*., 1986). Taken together, our data show that the effect of excess H_2 production on growth depends on its magnitude as well as the tradeoffs between electron availability, balancing and nitrogen acquisition during growth under different metabolic conditions.

Fixed relative electron fluxes through Nase and Rubisco

During diazotrophic, photoheterotrophic growth, the allocation of substrate-derived electrons between biomass, H_2 and CO_2 reflects the total electron fluxes through Nase and Rubisco (Fig. 1). Nase functions in both nitrogen acquisition and electron balance, while the primary role of CO_2 fixation during photoheterotrophic growth is as an electron sink (Hallenbeck *et al*., 1990; Falcone and Tabita, 1991; Hädicke *et al*., 2011; Farmer *et al*., 2014; Gordon and McKinlay, 2014). Total electron flux through Nase and Rubisco increases with the growth rate for the wild type, Mo-Nase and V-Nase strains, but is always high for the Fe-Nase strain (Fig. 4C and Fig. S9). The addition of the exogenous electron acceptor dimethyl sulfoxide (DMSO, 40 mM) removes the growth rate differences between the Mo-Nase and V-Nase mutant strains (Fig. 2B), indicating the use of the V-Nase isoform as an electron sink can promote growth.

Strikingly, despite large differences (up to ~1.75-fold) in growth rate and biomass nitrogen content between strains (Fig. 3), the relative electron fluxes through Nase and Rubisco remain constant, averaging ~60% Nase for all strains (Table 3). This means that the electron supply from the substrate is allocated at fixed proportions to Nase and Rubisco irrespective of growth rates and the extent of biomass nitrogen limitation (Fig. 3). This observation suggests that, as long as both proteins are present, cellular metabolites like ATP or electron carriers, involved in energy metabolism rather than nutrient status, control the relative rates of carbon and nitrogen fixation in photoheterotrophic *R. palustris*. It is unclear why biomass nitrogen limitation, as is the case for the Fe-Nase strain on both carbon substrates, does not result in the reallocation of electrons from Rubisco to Nase. This result suggests that, for photoheterotrophy, there could be selective pressures to maintain a carbon fixation flux even at the expense of nitrogen acquisition and growth rate.

Growth rate differences are associated with widespread proteomic changes beyond Nase isoform

The Nase isoforms are often described in a hierarchy, where the alternative V- and Fe-Nases act as back-up enzymes to the Mo-Nase to sustain diazotrophic growth, albeit at slower rates, when Mo becomes limiting (e.g. Oda *et al*., 2005; Hamilton *et al*., 2011; Darnajoux *et al*., 2017). From a regulatory perspective, this is compatible with our data: the wild type strain uses the Mo-Nase isoform under all the Mo-replete conditions we tested, regardless of the carbon substrate. However, our data show that the hierarchy in Nase usage is not

Table 3. Percentage of the reductive electron flux allocated to H_2 and Nase.

	Succinate		Acetate	
	%H_2 of Nase	%Nase of total	%H_2 of Nase	%Nase of total
Wild type strain	32 ± 8	63 ± 11	23 ± 6	64 ± 8
Mo-Nase strain	27 ± 6	63 ± 7	25 ± 5	58 ± 12
V-Nase strain	36 ± 13	56 ± 24	32 ± 12	59 ± 21
Fe-Nase strain	70 ± 8	55 ± 10	56 ± 6	45 ± 7

The proportion of the electron flux through Nase that is allocated to H_2 production varies among strains, but the relative electron flux through Nase rather than Rubisco remains fixed (~60%). Errors are SEs.

necessarily related to the isoforms' abilities to support fast growth under different conditions, because the V-Nase can support comparably fast growth on acetate. Conversely, fixing nitrogen exclusively with the Mo-Nase does not always yield fast growth, as is the case for the Mo-Nase mutant strain on acetate, which appears to suffer from an as yet undetermined metabolic deficiency.

To better understand how changes in Nase isoform usage are integrated with the broader physiology of N_2-fixing *R. palustris*, we examined the global protein expression patterns of all four strains in both carbon substrates. Interestingly, despite exclusive use of the Mo-Nase isoform by the wild type strain when grown on acetate, both its growth rate and proteome are more similar to that of the V-Nase strain than the Mo-Nase strain (Fig. 2 and Fig. S10, Table S4). The abundance of proteins related to coenzyme transport and metabolism (COG H) and energy production and conversion (COG C) in the wild type strain are also more similar to the V-Nase strain than the Mo-Nase strain on acetate (Fig. 2C). This shows that the observed differences in growth rates (Fig. 2) are associated with widespread proteomic changes and that many metabolic levers control nitrogen acquisition and diazotrophic fitness. Together the data imply that the effect of Nase isoform usage on growth is complex and may depend on *R. palustris*' ability to efficiently integrate a specific isoform into broader metabolic constraints under given growth conditions, rather than the Nase isoform properties alone. These results add nuance to the traditional view that use of the Mo-Nase is always more favorable for growth than the use of the V-Nase.

Conclusions

Contrary to the paradigm that diazotrophic growth with the Mo-Nase is inherently better than with the other Nase isoforms, we show that, for the bacterium *R. palustris*, use of the alternative V-Nase can support similar growth rates as use of the canonical Mo-Nase during N_2 fixing photoheterotrophic growth on acetate. The V-Nase strain can efficiently reduce N_2 and generate nitrogen replete biomass. At 19°C, its H_2:N_2 stoichiometry, around ~1.5, is only slightly higher than for the Mo-Nase strain (~1.0). During growth on acetate, excess H_2 production does not lead to slower V-Nase based growth compared with the Mo-Nase. From an evolutionary perspective, our results suggest that using the alternative V-Nase might not be as physiologically detrimental for organisms as has been assumed, decreasing the selective pressure to remove genes for this isoform from diazotroph genomes. Our results show that the effect of Nase isoform usage on physiology, growth rate and H_2 yield is more complex than previously recognized, and that our understanding of why alternative nitrogenases persist in nature requires consideration of broader metabolic constraints, including carbon substrates, environmental conditions, and metabolic integration of diazotrophy with phototrophy, heterotrophy and carbon fixation.

Experimental procedures

Bacterial cultures

Rhodopseudomonas palustris strains CGA009 (wild type), CGA753 ('Mo-Nase strain,' Mo-nitrogenase only, genotype: Δ*vnfH* Δ*anfH*), CGA766 ('V-Nase strain,' V-nitrogenase only, genotype: Δ*nifH nifD::Tn5* Δ*anfA*) and CGA755 ('Fe-Nase strain,' Fe-nitrogenase only, genotype: Δ*nifH* Δ*vnfH*) were grown in batch cultures at 19°C and ~90 μmols photons m^{-2} s^{-1} under anaerobic photoheterotrophic conditions in defined nitrogen-fixing medium with 2.5 μM Fe, 100 nM Mo, 10 μM V, Wolfe's vitamin solution, 0.0005% yeast extract and either 10 mM succinate, 20 mM acetate, or a mixture of 10 mM butyrate and 5 mM sodium bicarbonate (Oda *et al*., 2005; Zhang *et al*., 2014). We used genetic mutants because Mo limitation is difficult to achieve, and even residual Mo can result in the presence of some Mo-nitrogenase (Jacobitz and Bishop, 1992; Kimble and Madigan, 1992; Bellenger *et al*., 2008, 2011; Sippel *et al*., 2017). In *R. palustris* CGA009, the V- and Fe-Nase isoforms are regulated by nitrogen status rather than metal availability, allowing these mutants to grow despite the presence of ample Mo (Oda *et al*., 2005). Where applicable, the final concentration of dimethyl sulfoxide (DMSO, Sigma Life Science, Bio Reagent Grade) was 40 mM. The culture media were prepared in an anaerobic glove box (COY Laboratory Products) in lieu of the Hungate technique, leading to a headspace composition of N_2 with a background level of ~2% v/v H_2. Oxygen was removed by microwaving, vacuum sonicating, and allowing the medium to sit in glove bag for several days until dissolved O_2 was below the detection limit of our O_2 probe (Hach HQ40d portable meter with LDO101 rugged optical dissolved oxygen probe, range 0.1–20 mg L^{-1} corresponding to 1%–200% saturation). Bacterial growth was monitored by optical density (OD_{660}) using a Spectronic 20D+ (Thermo Fisher Scientific) or a Genesys 20 visible spectrophotometer (Thermo Fisher Scientific) and converted to cell density using the empirically observed relationship cells $ml^{-1} = 2.29 \times 10^9 \times OD_{660}$.

Biomass composition

Cultures were subsampled anaerobically during exponential growth (OD_{660} ~ 0.35–0.75). Bacterial biomass was collected either on combusted glass fiber filters, washed with 10 mL milli-Q water, and dried overnight at

60°C, or by pelleting and freeze-drying, which yielded statistically indistinguishable results. A vario ISOTOPE select (Elementar Isoprime) was used to quantify total carbon, nitrogen, and biomass $\delta^{13}C$ and $\delta^{15}N$. Measurements were calibrated with an in-house aminocaproic acid standard (ACROS) and validated using the USGS 40 standard. Biomass CHNO composition was measured using a TruSpec Micro (LECO) and was, on average, $CH_{1.75}N_{0.18}O_{0.54}$.

Analytical techniques

Headspace H_2 and CO_2 were sampled periodically throughout growth and in early stationary phase. In early experiments, samples were diluted 10-fold and H_2 and CO_2 were quantified simultaneously using gas chromatography with thermal conductivity and flame ionization detectors (TCD and FID Peak Performer 1 series, Peak Laboratories) using a methanizer to convert CO_2 into CH_4 and UHP argon as a carrier gas. In later experiments, H_2 and CO_2 were measured simultaneously in undiluted samples using gas chromatography with a thermal conductivity detector (GC-8AIT TCD, Shimadzu Instruments; detector temperature = 150°C, column temperature = 100°C) and the Restek ShinCarbon ST column with UHP nitrogen as a carrier gas. Dissolved CO_2 was quantified by injecting 500 or 200 µl of culture into a sealed, N_2-flushed 27 ml anaerobic culture tube resp. 10 ml amber vial containing 0.1 ml of 12 N HCl, vortexing for 30 s, and allowing the sample to equilibrate for at least 15 min before the headspace was sampled (McKinlay and Harwood, 2010a). Total CO_2 was calculated as the sum of the measured headspace CO_2 and dissolved inorganic carbon.

N_2 and CO_2 fixation rates

N_2 and CO_2 fixation rates were measured in dual $^{15}N_2$ $H^{13}CO_3^-$ tracer experiments. As described in Mohr and colleagues (2010), $^{15}N_2$ enriched medium was prepared by replacing the headspace of 30 ml serum vials, which had been pre-filled with 25 ml of anaerobic nitrogen-fixing medium, with Ar gas, degassing with a vacuum handpump, and injecting an overpressure of $^{15}N_2$ gas (98%+, Cambridge Isotope Laboratories, Andover, MA, USA). The bottles were shaken for >5 days, the overpressure was removed, and they were allowed to equilibrate until the experiment. The 0.5 M ^{13}C-bicarbonate stock was prepared in 5 ml amber serum vials by adding the bicarbonate stock (99%, Aldrich Chemistry), flushing with N_2, evacuating the headspace with a handpump, and filling the vial completely with sterile growth medium. Pre-grown cultures (10 ml in 27 ml Balch Tubes; OD_{660} ~0.3–0.5) were spiked with 1 ml of the $^{15}N_2$ saturated medium, 100 µl of the ^{13}C-bicarbonate stock, and 10% $^{15}N_2$ gas was added to the headspace. Every hour for 3 h, cells were filtered onto combusted GF/F filters (Whatman, GE Healthcare Life Sciences) and analyzed for their $^{15}N^{13}C$ content by isotope ratio mass spectrometry at the Stable Isotope Facility (UC Davis). Using the measured stoichiometry, electron fluxes through Nase and Rubisco were calculated by assuming six electrons per N_2 reduced, two electrons per H_2 produced, and 4.13 electrons per CO_2 fixed.

Proteomics

R. palustris cell pellets were extracted by heating (95°C, 20 min) and vortexing in a reducing and denaturing SDS (1%)/Tris(200 mM, pH 8.0)/DTT(10 mM) buffer, and cysteine thiols alkylated with 40 mM iodoacetamide. Proteins were purified by a modified eFASP (enhanced filter-aided sample preparation) protocol (Erde *et al*., 2014), using Sartorius Vivacon 500 concentrators (30 kDa nominal cutoff). Proteins were digested with MS-grade trypsin (37°C, overnight), and peptides were eluted from the concentrator dried by vacuum centrifugation. For quantitative analysis, peptides were isotopically labelled at both N- and C-termini using the diDO-IPTL methodology (Waldbauer *et al*., 2017). Briefly, C-termini were labelled with either oxygen-16 or -18 by enzymatic exchange in isotopic water of >98 atom% enrichment. N-termini were labelled with either un- or di-deuterated formaldehyde via reductive alkylation using sodium cyanoborohydride. Peptide extracts from each sample were split and aliquots labelled separately with $CD_2O/^{16}O$ and $CH_2O/^{18}O$; the latter were pooled to serve as a common internal standard for quantification. Aliquots of the ^{16}O-labelled peptides and ^{18}O-labelled internal standard were mixed 1:1 v/v and analysed by LC–MS for protein expression quantification.

For LC–MS analysis, peptide samples were separated on a monolithic capillary C18 column (GL Sciences Monocap Ultra, 100 µm I.D. × 200 cm length) using a water-acetonitrile +0.1% formic acid gradient (2%–50% AcN over 180 min) at 360 nl min^{-1} using a Dionex Ultimate 3000 LC system with nanoelectrospray ionization (Proxeon Nanospray Flex source). Mass spectra were collected on an Orbitrap Elite mass spectrometer (Thermo) operating in a data-dependent acquisition mode, with one high-resolution (120 000 $m/\Delta m$) MS1 parent ion full scan triggering Rapid-mode 15 MS2 CID fragment ion scans of selected precursors. Proteomic mass spectral data were analysed using MorpheusFromAnotherPlace (MFAP; Waldbauer *et al*., 2017), using the predicted proteome of *R. palustris* CGA009 as a search database. Precursor and product ion mass tolerances for MFAP searches were set to 20 ppm and 0.6 Da respectively. Static cysteine

carbamidomethylation and variable methionine oxidation, N-terminal (d4)-dimethylation and C-terminal $^{18}O_2$ were included as modifications. The false discovery rate for peptide-spectrum matches was controlled by target-decoy searching to <0.5%. For Nase proteins with high homology between isoforms, the spectra were additionally manually curated to ensure that peptide assignments were unique and not due to contamination. Protein-level relative abundances and standard errors were calculated in R using the Arm postprocessing scripts for diDO-IPTL data (Waldbauer *et al*., 2017; github.com/waldbauerlab).

Proteomics analysis

The log2 effect was calculated as the log2 difference over the sum of the errors for both treatments and used to calculate the Bonferroni corrected *p*-value for significant differences from the Excel standard normal distribution function (norm.s.dist, cumulative = false). COG assignments were taken from UniProt on March 13, 2019, and hierarchical clustering was performed using the Morpheus Software from the Broad Institute (https://software.broadinstitute.org/morpheus) with the one minus Spearman Rank Correlation metric, average linkage method, and clustering by strain and carbon substrate treatment.

ACKNOWLEDGEMENTS

The Harwood lab (University of Washington) generously provided the bacterial strains used here. Yasuhiro Oda and Yanning Zheng provided valuable advice on culturing the V- and Fe-Nase strains and Kieran Pechter provided valuable advice on the proteomic analysis. Carol Chui collected preliminary data that informed the study. We thank Pauline Le Moinier and Jean-Philippe Bellenger for measuring CHNO biomass composition; Tullis Onstott for the use of Peak lab gas chromatographs; François Morel, Darcy McRose, Jessica Lueders-Dumont, and Romain Darnajoux for analytical help and/or useful discussions. This research was funded by the National Science Foundation (Award Number 1631814 to XZ and AMLK), an NSF Graduate Research Fellowship to KEL, the Simons Foundation (Award Number 402971 to JRW), and the Princeton Environmental Institute.

References

Alsiyabi, A., Immethun, C.M., and Saha, R. (2019) Modeling the interplay between photosynthesis, CO_2 fixation, and the quinone pool in a purple non-sulfur bacterium. *Sci Rep* **9**: 12638.

Andersen, K., and Shanmugam, K.T. (1977) Energetics of biological nitrogen fixation: determination of ratio of formation of H_2 to NH_4^+ catalyzed by nitrogenase of *Klebsiella pneumoniae* in vivo. *J Gen Microbiol* **103**: 107–122.

Bellenger, J.P., Wichard, T., and Kraepiel, A.M.L. (2008) Vanadium requirements and uptake kinetics in the dinitrogen-fixing bacterium *Azotobacter vinelandii*. *Appl Environ Microbiol* **74**: 1478–1484.

Bellenger, J.-P., Wichard, T., Xu, Y., and Kraepiel, A.M.L. (2011) Essential metals for nitrogen fixation in a free-living N_2-fixing bacterium: chelation, homeostasis and high use efficiency. *Environ Microbiol* **13**: 1395–1411.

Betancourt, D.A., Loveless, T.M., Brown, J.W., and Bishop, P.E. (2008) Characterization of diazotrophs containing Mo-independent nitrogenases, isolated from diverse natural environments. *Appl Environ Microbiol* **74**: 3471–3480.

Bishop, P.E., Hawkins, M.E., and Eady, R.R. (1986) Nitrogen fixation in molybdenum-deficient continuous culture by a strain of *Azotobacter vinelandii* carrying a deletion of the structural genes for nitrogenase (nifHDK). *Biochem J* **238**: 437–442.

Carlozzi, P., and Sacchi, A. (2001) Biomass production and studies on *Rhodopseudomonas palustris* grown in an outdoor, temperature controlled, underwater tubular photobioreactor. *J Biotechnol* **88**: 239–249.

Darnajoux, R. (2015) Étude de l'homéostasie des micronutriments de la fixation d'azote au sein de la symbiose lichénique en forêt boréale. PhD Thesis. Quebec, Canada: Université de Sherbrooke.

Darnajoux, R., Magain, N., Renaudin, M., Lutzoni, F., Bellenger, J.-P., and Zhang, X. (2019) Molybdenum threshold for ecosystem scale alternative vanadium nitrogenase activity in boreal forests. *Proc Natl Acad Sci USA* **116**: 24682–24688.

Darnajoux, R., Zhang, X., McRose, D.L., Miadlikowska, J., Lutzoni, F., Kraepiel, A.M.L., and Bellenger, J.-P. (2017) Biological nitrogen fixation by alternative nitrogenases in boreal cyanolichens: importance of molybdenum availability and implications for current biological nitrogen fixation estimates. *New Phytol* **213**: 680–689.

Demtröder, L., Narberhaus, F., and Masepohl, B. (2019) Coordinated regulation of nitrogen fixation and molybdate transport by molybdenum. *Mol Microbiol* **111**: 17–30.

Dick, J.M. (2014) Average oxidation state of carbon in proteins. *J R Soc Interface* **11**: 20131095.

Dilworth, M.J., Eldridge, M.E., and Eady, R.R. (1993) The molybdenum and vanadium nitrogenases of *Azotobacter chroococcum*: effect of elevated temperature on N_2 reduction. *Biochem J* **289**: 395–400.

Dos Santos, P.C., Fang, Z., Mason, S.W., Setubal, J.C., and Dixon, R. (2012) Distribution of nitrogen fixation and nitrogenase-like sequences amongst microbial genomes. *BMC Genomics* **13**: 162.

Eady, R.R. (1996) Structure-function relationships of alternative nitrogenases. *Chem Rev* **96**: 3013–3030.

Erde, J., Loo, R.R.O., and Loo, J.A. (2014) Enhanced FASP (eFASP) to increase proteome coverage and sample recovery for quantitative proteomic experiments. *J Proteome Res* **13**: 1885–1895.

Falcone, D.L., and Tabita, F.R. (1991) Expression of endogenous and foreign ribulose 1,5-bisphosphate carboxylase-oxygenase (RubisCO) genes in a RubisCO deletion mutant of *Rhodobacter sphaeroides*. *J Bacteriol* **173**: 2099–2108.

Farmer, R.M., Laguna, R., Panescu, J., McCoy, A., Logsdon, B., Zianni, M., *et al*. (2014) Altered residues in key proteins influence the expression and activity of the nitrogenase complex in an adaptive CO_2 fixation-deficient mutant strain of *Rhodobacter sphaeroides*. *Microbiology* **160**: 198–208.

Fixen, K.R., Oda, Y., and Harwood, C.S. (2019) Redox regulation of a light-harvesting antenna complex in an anoxygenic phototroph. *MBio* **10**: e02838–e02819.

Fixen, K.R., Pal Chowdhury, N., Martinez-Perez, M., Poudel, S., Boyd, E.S., and Harwood, C.S. (2018) The path of electron transfer to nitrogenase in a phototrophic alpha-proteobacterium. *Environ Microbiol* **20**: 2500–2508.

Glazer, A.N., Kechris, K., and Howard, J.B. (2015) Distribution and ecological niches of nitrogenases. In *Biol Nitrogen Fixat*. Vol. 1. de Bruijn, FJ (ed). 87–98.

Gollan, U., Schneider, K., Müller, A., Schüdderkopf, K., and Klipp, W. (1993) Detection of the in vivo incorporation of a metal cluster into a protein. *Eur J Biochem* **215**: 25–35.

Gordon, G.C., and McKinlay, J.B. (2014) Calvin cycle mutants of photoheterotrophic purple nonsulfur bacteria fail to grow due to an electron imbalance rather than toxic metabolite accumulation. *J Bacteriol* **196**: 1231–1237.

Gosse, J.L., Engel, B.J., Hui, J.C.H., Harwood, C.S., and Flickinger, M.C. (2010) Progress toward a biomimetic leaf: 4,000 h of hydrogen production by coating-stabilized nongrowing photosynthetic *Rhodopseudomonas palustris*. *Biotechnol Prog* **26**: 907–918.

Großkopf, T., and LaRoche, J. (2012) Direct and indirect costs of dinitrogen fixation in *Crocosphaera watsonii* WH8501 and possible implications for the nitrogen cycle. *Front Microbiol* **3**: 236.

Hädicke, O., Grammel, H., and Klamt, S. (2011) Metabolic network modeling of redox balancing and biohydrogen production in purple nonsulfur bacteria. *BMC Syst Biol* **5**: 150.

Hallenbeck, P.L., Lerchen, R., Hessler, P., and Kaplan, S. (1990) Roles of CfxA, CfxB, and external electron acceptors in regulation of ribulose 1,5-bisphosphate carboxylase/oxygenase expression in *Rhodobacter sphaeroides*. *J Bacteriol* **172**: 1736–1748.

Hamilton, T.L., Ludwig, M., Dixon, R., Boyd, E.S., Dos Santos, P.C., Setubal, J.C., *et al*. (2011) Transcriptional profiling of nitrogen fixation in *Azotobacter vinelandii*. *J Bacteriol* **193**: 4477–4486.

Harris, D.F., Lukoyanov, D.A., Kallas, H., Trncik, C., Yang, Z.-Y., Compton, P., *et al*. (2019) Mo-, V-, and Fe-nitrogenases use a universal eight-electron reductive-elimination mechanism to achieve N_2 reduction. *Biochemistry* **58**: 3293–3301.

Harris, D.F., Lukoyanov, D.A., Shaw, S., Compton, P., Tokmina-Lukaszewska, M., Bothner, B., *et al*. (2018a) Mechanism of N_2 reduction catalyzed by Fe-nitrogenase involves reductive elimination of H_2. *Biochemistry* **57**: 701–710.

Harris, D.F., Yang, Z.Y., Dean, D.R., Seefeldt, L.C., and Hoffman, B.M. (2018b) Kinetic understanding of N_2 reduction versus H_2 evolution at the E4 (4H) Janus state in the three Nitrogenases. *Biochemistry* **57**: 5706–5714.

Hillmer, P., and Gest, H. (1977) H_2 metabolism in the photosynthetic bacterium *Rhodopseudomonas capsulata*: H_2 production by growing cultures. *J Bacteriol* **129**: 724–731.

Hodkinson, B.P., Allen, J.L., Forrest, L.L., Goffinet, B., Sérusiaux, E., Andrésson, Ó.S., *et al*. (2014) Lichen-symbiotic cyanobacteria associated with *Peltigera* have an alternative vanadium-dependent nitrogen fixation system. *Eur J Phycol* **49**: 11–19.

Inomura, K., Bragg, J., and Follows, M.J. (2016) A quantitative analysis of the direct and indirect costs of nitrogen fixation: a model based on *Azotobacter vinelandii*. *ISME J* **11**: 166.

Jacobitz, S., and Bishop, P.E. (1992) Regulation of nitrogenase-2 in *Azotobacter vinelandii* by ammonium, molybdenum, and vanadium. *J Bacteriol* **174**: 3884–3888.

Jacobson, M.R., Premakumar, R., and Bishop, P.E. (1986) Transcriptional regulation of nitrogen fixation by molybdenum in *Azotobacter vinelandii*. *J Bacteriol* **167**: 480–486.

Kimble, L.K., and Madigan, M.T. (1992) Evidence for an alternative nitrogenase in *Heliobacterium gestii*. *FEMS Microbiol Lett* **100**: 255–260.

Krahn, E., Schneider, K., and Müller, A. (1996) Comparative characterization of H_2 production by the conventional Mo nitrogenase and the alternative "iron-only" nitrogenase of *Rhodobacter capsulatus* hup$^-$ mutants. *Appl Microbiol Biotechnol* **46**: 285–290.

Larimer, F.W., Chain, P., Hauser, L., Lamerdin, J., Malfatti, S., Do, L., *et al*. (2004) Complete genome sequence of the metabolically versatile photosynthetic bacterium *Rhodopseudomonas palustris*. *Nat Biotechnol* **22**: 55–61.

Lukoyanov, D., Khadka, N., Yang, Z.-Y., Dean, D.R., Seefeldt, L.C., and Hoffman, B.M. (2016) Reductive elimination of H_2 activates nitrogenase to reduce the N≡N triple bond: characterization of the E4 (4H) Janus intermediate in wild-type enzyme. *J Am Chem Soc* **138**: 10674–10683.

Lukoyanov, D., Yang, Z.-Y., Khadka, N., Dean, D.R., Seefeldt, L.C., and Hoffman, B.M. (2015) Identification of a key catalytic intermediate demonstrates that nitrogenase is activated by the reversible exchange of N_2 for H_2. *J Am Chem Soc* **137**: 3610–3615.

Luque, F., and Pau, R.N. (1991) Transcriptional regulation by metals of structural genes for *Azotobacter vinelandii* nitrogenases. *Mol Gen Genet* **227**: 481–487.

McCully, A.L., and McKinlay, J.B. (2016) Disrupting Calvin cycle phosphoribulokinase activity in *Rhodopseudomonas palustris* increases the H_2 yield and specific production rate proportionately. *Int J Hydrogen Energy* **41**: 4143–4149.

McCully, A.L., Onyeziri, M.C., LaSarre, B., Gliessman, J.R., and McKinlay, J.B. (2019) Reductive tricarboxylic acid cycle enzymes and reductive amino acid synthesis pathways contribute to electron balance in a *Rhodospirillum rubrum* Calvin-cycle mutant. *Microbiology*: 1-13.

McKinlay, J.B., and Harwood, C.S. (2010a) Carbon dioxide fixation as a central redox cofactor recycling mechanism in bacteria. *Proc Natl Acad Sci U S A* **107**: 11669–11675.

McKinlay, J.B., and Harwood, C.S. (2010b) Photobiological production of hydrogen gas as a biofuel. *Curr Opin Biotechnol* **21**: 244–251.

McKinlay, J.B., and Harwood, C.S. (2011) Calvin cycle flux, pathway constraints, and substrate oxidation state bacteria. *MBio* **2**: 1–9.

McRose, D.L., Zhang, X., Kraepiel, A.M.L., and Morel, F.M. M. (2017) Diversity and activity of alternative nitrogenases

in sequenced genomes and coastal environments. *Front Microbiol* **8**: 267.
Miller, R.W., and Eady, R.R. (1988) Molybdenum and vanadium nitrogenases of *Azotobacter chroococcum*: low temperature favors N_2 reduction by vanadium nitrogenase. *Biochem J* **256**: 429–432.
Mohr, W., Großkopf, T., Wallace, D.W.R., and LaRoche, J. (2010) Methodological underestimation of oceanic nitrogen fixation rates. *PLoS One* **5**: e12583.
Muller, F.M. (1933) On the metabolism of the purple sulphur bacteria in organic media. *Arch Microbiol* **4**: 131–166.
Mus, F., Alleman, A.B., Pence, N., Seefeldt, L.C., and Peters, J.W. (2018) Exploring the alternatives of biological nitrogen fixation. *Metallomics* **10**: 523–538.
Oda, Y., Wu, L., Liu, X., Yan, T., Zhou, J., Harwood, C.S., *et al*. (2005) Functional genomic analysis of three nitrogenase isozymes in the photosynthetic bacterium *Rhodopseudomonas palustris*. *J Bacteriol* **187**: 7784–7794.
Rey, F.E., Oda, Y., and Harwood, C.S. (2006) Regulation of uptake hydrogenase and effects of hydrogen utilization on gene expression in *Rhodopseudomonas palustris*. *J Bacteriol* **188**: 6143–6152.
Robson, R.L., Eady, R.R., Richardson, T.H., Miller, R.W., Hawkins, M., and Postgate, J.R. (1986) The alternative nitrogenase of *Azotobacter chroococcum* is a vanadium enzyme. *Nature* **322**: 388–390.
Schneider, K., Gollan, U., Dröttboom, M., Selsemeier-Voigt, S., and Müller, A. (1997) Comparative biochemical characterization of the iron-only nitrogenase and the molybdenum nitrogenase from *Rhodobacter capsulatus*. *Eur J Biochem* **244**: 789–800.
Schneider, K., Müller, A., Schramm, U., and Klipp, W. (1991) Demonstration of a molybdenum- and vanadium-independent nitrogenase in a nifHDK-deletion mutant of *Rhodobacter capsulatus*. *Eur J Biochem* **195**: 653–661.
Schubert, K.R., and Evans, H.J. (1976) Hydrogen evolution: a major factor affecting the efficiency of nitrogen fixation in nodulated symbionts. *Proc Natl Acad Sci U S A* **73**: 1207–1211.
Simpson, F.B., and Burris, R.H. (1984) A nitrogen pressure of 50 atmospheres does not prevent evolution of hydrogen by nitrogenase. *Science* **224**: 1095–1097.
Sippel, D., Schlesier, J., Rohde, M., Trncik, C., Decamps, L., Djurdjevic, I., *et al*. (2017) Production and isolation of vanadium nitrogenase from *Azotobacter vinelandii* by molybdenum depletion. *J Biol Inorg Chem* **22**: 161–168.
Waldbauer, J., Zhang, L., Rizzo, A., and Muratore, D. (2017) diDO-IPTL: a peptide-labeling strategy for precision qutative proteomics. *Anal Chem* **89**: 11498–11504.
Zhang, X., McRose, D.L., Darnajoux, R., Bellenger, J.P., Morel, F.M.M., and Kraepiel, A.M.L. (2016) Alternative nitrogenase activity in the environment and nitrogen cycle implications. *Biogeochemistry* **127**: 189–198.
Zhang, X., Sigman, D.M., Morel, F.M.M., and Kraepiel, A.M. L. (2014) Nitrogen isotope fractionation by alternative nitrogenases and past ocean anoxia. *Proc Natl Acad Sci U S A* **111**: 4782–4787.

Supporting Information

Additional Supporting Information may be found in the online version of this article at the publisher's web-site:

Appendix S1. Supporting Information figures, discussion, experimental procedures and Tables S1 and S4.

Table S2. This table summarizes the H_2:N_2 ratios available in the literature. Published H_2:N_2 ratios are highly variable. They appear to be lowest at lower temperatures, high Fe protein:MoFe resp. VFe resp. FeFe protein ratios and higher N_2 partial pressures. This table was generated from the references in Eady (1996) and by a literature review of the 497 publications which, as of May 23, 2019, had cited it. Except for Bishop, Hawkins and Eady (1986), no data from experiments with an uptake Hase are included. Only papers that measured H_2 production and N_2 fixation rates under the same atmospheric composition are included.

Table S3. This excel document contains the data used in this publication.